# Overtaking-Enabled Eco-Approach Control at Signalized Intersections for Connected and Automated Vehicles

Haoxuan Dong<sup>®</sup>, Weichao Zhuang<sup>®</sup>, Member, IEEE, Guoyuan Wu<sup>®</sup>, Senior Member, IEEE, Zhaojian Li<sup>®</sup>, Senior Member, IEEE, Guodong Yin<sup>®</sup>, Senior Member, IEEE, and Ziyou Song, Senior Member, IEEE

Abstract—Preceding vehicles typically dominate the movement of following vehicles in traffic systems, thereby significantly influencing the efficacy of eco-driving control that concentrates on vehicle speed optimization. To potentially mitigate the negative effect of preceding vehicles on eco-driving control at the signalized intersection, this study proposes an overtakingenabled eco-approach control (OEAC) strategy. It combines driving lane planning and speed optimization for connected and automated vehicles to relax the first-in-first-out queuing policy at the signalized intersection, minimizing the host vehicle's energy consumption and travel delay. The OEAC adopts a two-stage receding horizon control framework to derive optimal driving trajectories for adapting to dynamic traffic conditions. In the first stage, the driving lane optimization problem is formulated as a Markov decision process and solved using dynamic programming, which takes into account the uncertain disturbance from preceding vehicles. In the second stage, the vehicle's speed trajectory with the minimal driving cost is optimized rapidly using Pontryagin's minimum principle to obtain the closed-form analytical optimal solution. Extensive simulations are conducted to evaluate the effectiveness of the OEAC. The results show that the OEAC is excellent in driving cost reduction over constant speed and regular eco-approach and departure strategies in various traffic scenarios, with an average improvement of 20.91% and 5.62%, respectively.

Index Terms— Eco-driving, connected and automated vehicles, Markov decision process, Pontryagin's minimum principle, lanechanging, speed optimization.

Manuscript received 11 April 2023; revised 5 August 2023; accepted 20 October 2023. Date of publication 7 November 2023; date of current version 13 May 2024. This work was supported in part by the A-Star Young Individual Research Grants (YIRG), Singapore, under Grant M22K3c0092; and in part by the U.S. National Science Foundation Award under Grant CMMI-2045436. The Associate Editor for this article was X. Hu. (Corresponding authors: Ziyou Song; Weichao Zhuang)

Haoxuan Dong and Ziyou Song are with the Department of Mechanical Engineering, National University of Singapore, Singapore 117575 (e-mail: donghaox@foxmail.com; ziyou@nus.edu.sg).

Weichao Zhuang and Guodong Yin are with the School of Mechanical Engineering, Southeast University, Nanjing 211189, China (e-mail: wezhuang@seu.edu.cn; ygd@seu.edu.cn).

Guoyuan Wu is with the Department of Electrical and Computer Engineering, University of California at Riverside, Riverside, CA 92507 USA (e-mail: guoyuan.wu@ucr.edu).

Zhaojian Li is with the Department of Mechanical Engineering, Michigan State University, East Lansing, MI 48824 USA (e-mail: lizhaoj1@egr.msu.edu).

Digital Object Identifier 10.1109/TITS.2023.3328022

# I. INTRODUCTION

HE growth of urbanization and the increasing vehicle ownership have led to an increase in the number of vehicles in urban traffic [1], [2], raising concerns about greenhouse gas emissions and traffic congestion [3]. Fortunately, by connecting vehicles and road infrastructure, the emerging connected and automated vehicle (CAV) technologies provide possibilities to further improve vehicle energy efficiency and traffic throughput [4], [5]. In this context, a variety of eco-friendly methods have been proposed from road or vehicle perspectives to improve energy efficiency and traffic efficiency. One such method is to optimize the traffic light signal phase and timing for prioritization of a single vehicle or a platoon approaching the intersection [6]. Another approach involves economically controlling the vehicle speed drive to pass through the intersection, known as eco-approach and departure (EAD) control in some literature [7].

The EAD utilizes look-ahead information on traffic lights and surrounding vehicles [7], [8], to facilitate smooth vehicle pass through signalized intersections and avoid stop-and-go behavior. A simple EAD is green light optimized speed advisory system, which uses deterministic traffic light signal phase and timing, speed limits, and vehicle kinematics to calculate the speed range that ensures the vehicle can pass through an intersection without stopping [9]. Considering the uncertain signal phase and timing of actuated traffic lights, Mahler and Vahidi [10] introduced a prediction model to determine the probability of green signals at each time step, then the vehicle energy-optimal speed trajectory was derived aiming to maximize the likelihood of passing through an intersection. In real-world traffic, the vehicle speed may be impacted by the preceding vehicle or the queue waiting at the intersection. Therefore, Hao et al. [8], Bai et al. [11], and Ye et al. [12] designed the EAD strategies considering preceding vehicle movement information obtained using onboard radar, vehicleto-vehicle communication, or prediction model. Dong et al. [13] and Sun et al. [14] proposed enhanced EAD to allow the vehicle to drive through the intersection without a stop by considering the discharging time of the vehicle queue, where the vehicle kinematics and traffic shockwave theory were utilized to estimate the vehicle queue movement. Other EAD

1558-0016 © 2023 IEEE. Personal use is permitted, but republication/redistribution requires IEEE permission. See https://www.ieee.org/publications/rights/index.html for more information.

strategies were proposed by Wang et al. [15], Han et al. [16], and Dong et al. [17]. These strategies are based on designing multiple intersection-based EAD controller that incorporates the spatial-temporal correlation among signalized corridors. Ma et al. [18], Li et al. [19], and Jiang et al. [20] proposed vehicle platoon-based EAD approaches aimed at improving the energy efficiency of multiple vehicles passing through the signalized intersection.

Most EAD research has focused on optimizing vehicle speed to control its longitudinal movement. However, the host vehicle (HV) may encounter slow-moving vehicles ahead in some scenarios. If the HV does not overtake the preceding vehicle, the HV speed optimization is restricted to the car-following mode, resulting in degraded efficacy of EAD control. Earlier vehicle overtaking research concentrated on lane-changing decision and trajectory optimization, Zhou et al. [21] and Li et al. [22] formulated optimal lane-changing strategies that consider HVs and other vehicles in their vicinity to improve driving comfort, safety, and lane-changing efficiency in complex driving environments. These studies, however, omit the vehicle energy-saving objective, which could lead to a reduction in vehicle energy efficiency when frequent lane changes are present. To address this issue, Gu et al. [23] and Dong et al. [24] developed a flexible eco-cruising strategy with efficient driving lane planning and speed optimization capabilities simultaneously for CAVs. Chen et al. [25] derived time and energy-optimal lane-changing control policies that cooperate with neighboring CAVs, the maneuver time subject to safety constraints and associated surrogate energy consumption of all cooperating vehicles was minimized.

The studies mentioned above focus on overtaking-enabled eco-cruising control on highways; however, the offered solutions may not apply to urban traffic due to the presence of traffic lights. Lane-changing in urban traffic is not only for achieving the goals of improving vehicle energy efficiency and reducing travel delay by considering the impact of preceding vehicles as in a highway scenario, but also to ensure vehicles pass through signalized intersections without stopand-go operation during the green window of traffic light. Currently, there are few investigations of overtaking-enabled EAD. Yang et al. [26] designed a less-disturbed EAD strategy that integrates offline energy-efficient speed planning and online speed tracking with overtaking ability. Nevertheless, the less-disturbed EAD does not achieve an energy-saving control globally since lane changing is not considered in vehicle speed planning. Guo et al. [27] developed a hybrid deep Q-learning and policy gradient-based EAD under a full CAVs environment, where both speed optimization and lane-changing order were considered. However, because the fully connected environment can only be realized in the distant future [28], [29] and the proposed approach does not take vehicle lane-changing trajectory into consideration, this approach is not practical in real-world traffic. Moreover, Hu et al. [30] proposed an enhanced EAD controller to cut through the traffic and catch green signals by overtaking slow-moving vehicles for real-time application in a partially connected environment. However, this study formulated a nonlinear optimal control problem based on

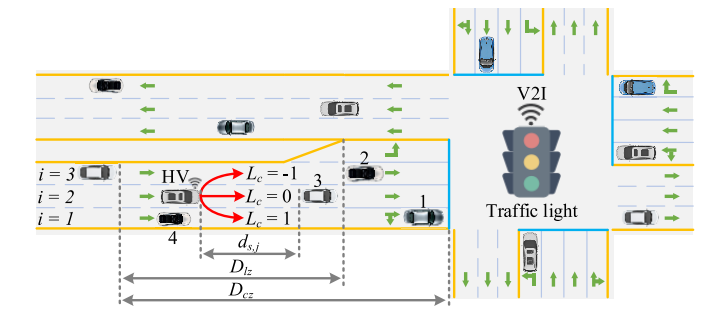


Fig. 1. A general signalized intersection route.

a simplified vehicle model that ignored the vehicle powertrain model. The resulting solution could be different from reality.

This study proposes an overtaking-enabled eco-approach control (OEAC) strategy for CAVs, which is capable of relaxing the first-in-first-out queuing policy at a signalized intersection, while minimizing vehicle energy consumption and travel delay in a computationally efficient manner. The major contributions are threefold:

- 1) An overtaking-enabled EAD optimal control problem is formulated to cooperate with driving lane planning and speed optimization while considering the constraints posed by traffic lights and preceding vehicles. The unified monetary counterpart objectives of energy consumption and travel time are used to balance vehicle energy and traffic efficiency.
- 2) A real-time optimal driving trajectory is derived through a two-stage receding horizon control framework. In the first stage, the driving lane decision is formulated as a Markov decision process (MDP), and dynamic programming is adopted to solve this problem while considering the uncertain disturbance of preceding vehicles. In the second stage, the speed trajectory is optimized using Pontryagin's minimum principle (PMP) algorithm with minimal driving costs, leading to rapid optimization.
- 3) The simulation of stochastic traffic scenarios and typical case studies are investigated to verify the effectiveness of the proposed OEAC strategy. Furthermore, the sensitivity of OEAC's effectiveness to traffic flow conditions and traffic light initial states is inspected.

The remainder of this paper is organized as follows. Section II formulates the intersection crossing scenario and vehicle model. In Section III, the EAD optimal control problem and the OEAC framework are defined. Section IV provides the methodology of the OEAC in detail. The performance of the OEAC is comprehensively evaluated in Section V. Finally, Section VI concludes this paper.

# II. INTERSECTION CROSSING SCENARIO AND VEHICLE MODEL

## A. Intersection Crossing Scenario

We consider a general three-lane urban route with a fixed-timing traffic light, as shown in Fig. 1.

The route is defined as a set  $\mathcal{O}_r = \{S_{tl}, D_{cz}, D_{lz}, N_l, D_w, V_{max}, V_{min}\}$ .  $S_{tl}$  is the location of the stop line at the intersection,  $D_{cz}$  is the communication zone,  $D_{lz}$  is the

lane-changing coordinator zone, which is related to  $D_{cz}$  and the length of no lane-changing zone near the intersection stop line.  $N_l$  is the total number of lanes in the same driving direction as the HV, where the lane numbers from the outside to the inside of the road are  $i=1,2,\cdots,N_l$ .  $D_w$  is the width of the lane, and  $V_{max}$  and  $V_{min}$  are maximum and minimum speed limits, respectively.

The information on traffic lights is defined by a set  $\mathcal{O}_t = \{T_{ls}, I_{in}, T_{gr}, T_{re}\}$ , where  $T_{ls}$  is the initial transition time of the traffic light indication when the HV is approaching the communication zone,  $I_{in}$  is the initial indication of the traffic light with  $I_{in} = 1$  and  $I_{in} = 0$  denoting the green and red signals, respectively, and  $T_{gr}$  and  $T_{re}$  are the time interval of green and red signals, respectively. Note that the yellow signal is lumped into the red for driving safety concerns.

The set of surrounding vehicles is given by  $\mathcal{O}_s = \{N_{sv}, s_{s,j}, v_{s,j}, L_{s,j}\}$ . Specifically,  $N_{sv}$  is the number of surrounding vehicles, where we specify vehicle serial numbers as  $j=1,2,\cdots,N_{sv}$ , in the order of proximity to the intersection and being from the innermost lane to the outermost lane.  $s_{s,j}$ ,  $v_{s,j}$ , and  $L_{s,j}$  are the position, speed, and driving lane of jth surrounding vehicle, respectively. The surrounding vehicle can be classified into three types by their relative position for the HV in the longitudinal direction: the vehicle in front of the HV is the preceding vehicle, the vehicle driving side by side with the HV is the side vehicle, and the vehicle behind the HV is the rear vehicles.

It is also assumed that the HV is equipped with a vehicle-to-infrastructure communication device (4G cellular network) and can access instantaneous traffic information. The HV can modify its speed in the communication zone and change the driving lane in the lane change coordinator zone. Note that the lane-changing rule is constructed to only permit the HV to drive in the current lane or change to the adjacent lanes, as shown in Fig. 1. Therefore, the maximum permissible lane shift is only one, and the lane-changing index  $L_c$  has only three values, i.e.,  $L_c = [-1, 0, 1]$ , corresponding to changing lanes to the left, driving in the current lane, and changing lanes to the right, respectively.

# B. Vehicle Model

When vehicles change lanes, we assume that the steering action is mild, the speed is moderate, and the wheels do not slip at their contact point with the ground, so the vehicle complies with the dynamics and movement geometry constraints. The bicycle model with an Ackerman steering design is used to explain vehicle lateral and longitudinal movements [30], as expressed in (1),

$$\begin{bmatrix} \dot{s_x} \\ \dot{s_y} \\ \dot{\gamma} \end{bmatrix} = \begin{bmatrix} \cos \gamma \\ \sin \gamma \\ \tan \beta_w / L \end{bmatrix} v \tag{1}$$

where v is the speed,  $\gamma$  is the yaw angle,  $\beta_w$  is the front-wheel steering angle, L is the vehicle body length, and  $s_x$  and  $s_y$  are the longitudinal and lateral positions, respectively.

We focus on the EAD control of an electric vehicle that is powered by a centralized electric motor. Ignoring the electric wire loss, the battery power is calculated by (2),

$$P_b = P_m \eta_b^{-\text{sign}(P_m)} + P_a \eta_b^{-1}$$
 (2)

where  $\eta_b$  is the battery efficiency,  $P_a$  is the vehicle accessory power, and  $P_m$  is the motor power. The approximated closed-form expression of motor power [31] is used to reduce the computational burden, as expressed in (3),

$$P_m = \varpi T_m v + \kappa T_m^2 \tag{3}$$

where  $\varpi$  and  $\kappa$  are the empirical coefficients, i.e.,  $\varpi = i_g i_0 / r_w$  and  $\kappa = R_m / \mu^2$ .  $R_m$  is the motor armature resistance,  $\mu$  is the motor speed constant, and  $T_m$  is the motor torque, as defined in (4) [32],

$$T_{m} = \frac{\left(mgf\cos\theta + mg\sin\theta + 0.5C_{D}A\rho v^{2} + m\delta\dot{v}\right)r_{w}}{i_{g}i_{0}\eta_{t}^{\text{sign}(T_{m})}} \tag{4}$$

where m is the vehicle mass, g is the gravity acceleration, f is the rolling resistance coefficient,  $C_D$  is the aerodynamic drag coefficient, A is the frontal area,  $\rho$  is the air density,  $\delta$  is the vehicle rotational inertia coefficient,  $r_w$  is the radius of the vehicle tire,  $i_g$  is the transmission ratio,  $i_0$  is the final drive ratio,  $\eta_t$  is the driveline efficiency,  $\theta$  is the road slope, and sign () is the signum function.

# III. PROBLEM FORMULATION AND CONTROL FRAMEWORK

### A. EAD Problem Analysis

EAD control is recognized as a promising approach to reducing vehicle energy consumption and travel delay at signalized intersections [4]. Regular EAD (READ) uses traffic light and preceding vehicle information, as shown in the blue solid line in Fig. 2, to calculate the speed to pass through the signalized intersection without stopping. While approaching the preceding vehicle, the HV must adhere to the first-in-first-out queuing policy, which may increase the travel time when encountering a slow-moving preceding vehicle. Additionally, due to the blocking effect of the preceding vehicle, the speed of READ may not be optimal.

In this context, to realize a more efficient vehicle control system, this study proposes an overtaking-enabled EAD strategy, referred to as OEAC, for safely and efficiently passing through the signalized intersection by combining driving lane planning and speed optimization. As shown in the green solid and dotted lines in Fig. 2, the HV with OEAC can overtake the slower vehicle, therefore relaxing the first-in-first-out queuing policy to reduce vehicle energy consumption and travel delay effectively.

# B. Optimization Control Problem

The objective of the proposed OEAC is to maneuver the vehicle efficiently passing through the signalized intersection with a minimal driving cost. The controller must determine the optimal driving lane and speed for the HV, considering relevant vehicle and traffic constraints, to reach the destination with the shortest amount of time and reduced energy consumption.

We define the state variable x as including vehicle speed and longitudinal position, i.e.,  $x = [v, s_x]^T$ . We assume

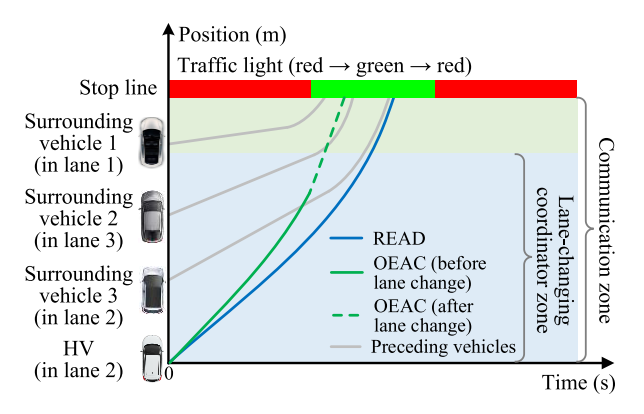


Fig. 2. Schematic diagram of a vehicle crossing the signalized intersection with READ and OEAC strategies. Here, the HV initially drives in lane 2 before changing to lane 1.

no mechanical brake force is actuated in order to increase the vehicle energy efficiency while taking into account the requirements for maximum deceleration and the available motor torque [33]. Then, the control inputu includes motor torque and lane-changing index, i.e.,  $u = [T_m, L_c]^T$ . Since the dimension of quantity in terms of energy consumption and travel time are not uniform [24], a monetary counterpart normalized objective of vehicle energy and travel time is established to calculate the driving cost. Consequently, the overtaking-enabled EAD optimal control problem is formulated in (5) and (6a), with the goal of minimizing driving cost (see (5)), under muti-constraints, i.e., speed limits (see (6a)), motor torque bounds (see (6b)), lane change integer constraint (see (6c)), safety intervehicle distance (see (6d)), traffic light control policy (see (6e)), and initial and final states constraints (see (6f)),

$$\min_{u \in U} \mathcal{J}(x, u) = \int_{T_{\varepsilon}}^{T_f} (\zeta_e P_b + \zeta_t) dt$$
 (5)

subject to: 
$$V_{min} \le v \le V_{max}$$
 (6a)

$$T_{mmin} \le T_m \le T_{mmax}$$
 (6b)

$$L_c \in [-1, 0, 1]$$
 (6c)

$$d_{s,j} - \delta_{s,j} \ge 0 \tag{6d}$$

$$\begin{cases} v = 0 & if s_x = S_{tl} - S_{ts} \text{ and } P = 0 \\ v \neq 0 & if s_x = S_{tl} - S_{ts} \text{ and } P = 1 \end{cases}$$
 (6e)

given: 
$$x(T_s) = [V_s, 0], s_x(T_f) = S_{tl}$$
 (6f)

where  $T_s$  is the initial time,  $T_f$  is the final time at which the HV reaches the destination, which is variable.  $\zeta_e$  and  $\zeta_t$  are coefficients that convert the electricity and time costs into their monetary counterpart, respectively.  $V_s$  and  $V_f$  are the vehicle's initial and final speeds, respectively.  $T_{mmin} < 0$  and  $T_{mmax} \ge 0$  are the motor maximum generation and propulsion torque, respectively.  $d_{s,j}$  is the distance between the HV and the jth vehicle.  $\delta_{s,j}$  is the minimum safe gap between the HV and the jth vehicle, which is defined by using an intelligent driver model [34].  $S_{ts}$  is the standstill space between HV and the intersection stop line. P is the traffic light indication, in the initial traffic light cycle  $P = I_{in}$ , following P is determined from the traffic light model [17].

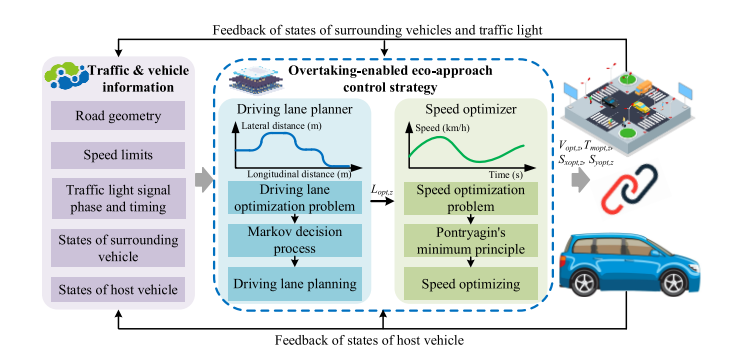


Fig. 3. The two-stage receding horizon control framework of the OEAC.

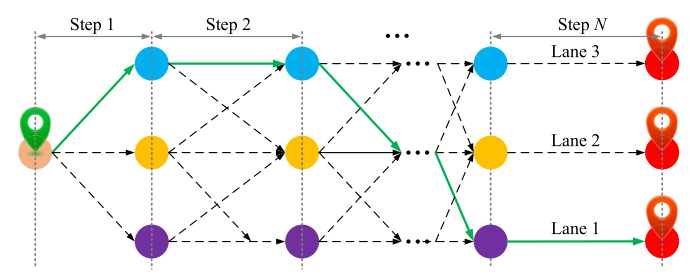


Fig. 4. A tree representation of the driving lane from God's eye point of view. Here the green solid and black dotted lanes donate the optimal and feasible driving lane sequences, respectively.

#### C. Control Framework

The overtaking-enabled EAD optimal control problem is a complicated nonlinear time-varying optimization problem with multiscale objectives and various types of constraints, which is difficult to solve directly. Furthermore, the states of the surrounding vehicles are dynamically changeable, and difficult to forecast properly, which significantly affects the EAD control performance.

As a result, this study proposes OEAC with a two-stage receding horizon control framework (see Fig. 3): the driving lane and speed are optimized in the first and second stages, respectively. Then, the overtaking-enabled EAD optimal control problem can be decomposed into driving lane planning and speed optimization problems, and solved using MDP theory and PMP algorithm, respectively. Benefitting from the efficient optimization algorithm and receding horizon control framework, the OEAC is able to calculate the vehicle optimal driving trajectory in real-time and adapt to dynamic traffic conditions.

# IV. OVERTAKING-ENABLED ECO-APPROACH CONTROL STRATEGY

# A. Efficient Driving Lane Planning

1) Driving Lane Optimization Problem: Fig. 4 illustrates a tree graph to represent how the vehicle changes lanes while driving. The entire trip may be segmented into N steps in the spatial domain, each of which necessitates choosing whether to change lanes or stay in the same lane. In lane-changing and lane-keeping operations, the travel period  $\Delta t_z$ , longitudinal distance interval  $\Delta s_{x,z}$ , and lateral distance interval  $\Delta s_{y,z}$  are different. Note that the subscript z = 1, 2, ..., N indicates the receding optimization step numbers.

This study employs a receding horizon framework and assumes that the HV lane-changing operation continues once

it begins until it enters the target lane. Given the state variable  $x_{l,z} = [t_z, s_{x,z}, s_{y,z}]$  and control input  $u_{l,z} = L_{c,z}$ . Then, the driving lane optimization problem is formulated in (7),

$$\min_{u_{l,z} \in U} \mathcal{J}_{l} (x_{l,z}, u_{l,z}) = \sum_{z=1}^{N} (\zeta_{e} P_{b,z} + \zeta_{t}) \Delta t_{z}$$
subject to:  $L_{c,z} \in [-1, 0, 1]$ 

$$d_{s,j,z} - \delta_{s,j,z} \ge 0$$

$$x_{l,z+1} = \begin{bmatrix} t_{z+1} \\ s_{x,z+1} \\ s_{y,z+1} \end{bmatrix} = \begin{bmatrix} t_{z} + \Delta t_{z} \\ s_{x,z} + \Delta s_{x,z} \\ s_{y,z} + \Delta s_{y,z} \end{bmatrix} \tag{7}$$

where  $\Delta t_z \in \{\Delta t_{c,z}, \Delta t_{k,z}\}$ ,  $\Delta s_{x,z} \in \{\Delta s_{xc,z}, \Delta s_{xk,z}\}$ , and  $\Delta s_{y,z} \in \{s_{yc,z}, \Delta s_{yk,z}\}$ .  $\Delta t_{c,z}$  and  $\Delta t_{k,z}$  are time intervals of lane-changing and lane-keeping, respectively.  $\Delta s_{xc,z}$  and  $\Delta s_{xk,z}$  denote the longitudinal distances of lane-changing and lane-keeping, respectively.  $s_{yc,z}$  and  $\Delta s_{yk,z}$  are the lateral distances of lane-changing and lane-keeping, respectively. Then  $\Delta t_{c,z} = \Delta s_{cx,z}/V_{h,z}$  and  $\Delta t_{k,z} = \Delta s_{kx,z}/V_{h,z}$ , where  $V_{h,z}$  is the speed of HV at the beginning of zth step. Note that  $\Delta t_z$ ,  $\Delta s_{xc,z}$ , and  $\Delta s_{yc,z}$  are related to lane-changing trajectories. Here we choose the third-order polynomial based lane-changing trajectory model [24], which has the advantages of a closed form and smooth curvature.

2) Safety Concerns During Lane-Changing: The operation of changing lanes offers a larger risk to safety than lane-keeping because the lateral displacement of the vehicle during lane-changing disrupts the flow of traffic in the adjacent lanes. The potential collision scenarios in the target lane can be categorized into two groups: rear-end collision caused by a slower preceding vehicle or a faster rear vehicle; and side collision attributable to the side vehicle driving at the same speed as the HV. We define the flags that allow HV changes to the left or right lanes as  $\psi_{cl}$  and  $\psi_{cr}$ , respectively, and the values 1 and 0 indicate that the lane can and cannot be changed. Then, the safety lane-changing criteria are summarized in (8).

$$L_{c,z} = \begin{cases} -1 & \psi_{cl,z} = 1\\ 0 & \psi_{cl,z} = 0 \text{ and } \psi_{cr,z} = 0\\ 1 & \psi_{cr,z} = 1 \end{cases}$$
 (8)

The lane-changing flags are determined by the safety clearance between HV and the nearest preceding, rear, or side vehicles, which is calculated by geometric methods [34], as given in (9),

$$\delta_{s,j,z} = H_s + \max\left(0, T_h v_z + \frac{v_z \left(v_z - v_{s,j,z}\right)}{2\sqrt{a_{min}a_{max}}}\right) \tag{9}$$

where  $H_s$  is the standstill distance between the HV and the nearest vehicle,  $T_h$  is the safety time headway,  $v_{s,j,z}$  is the speed of the nearest surrounding vehicles, and  $a_{min}$  and  $a_{max}$  are maximum deceleration and acceleration considering driving comfort, respectively.

3) Efficient Driving Lane Planning Using MDP Theory: The movement of surrounding vehicles greatly influences the lane-changing decision of HV. Most research on lane-changing control assumes the movement of surrounding vehicles can be

accurately accessed [21] or predicted [26]. However, accurate prediction is more challenging because of the random behaviors of surrounding vehicles. In this context, this study employs MDP to find the optimal driving lane considering the uncertainties of surrounding vehicles.

The driving lane optimization problem is a deterministic problem, which is transformed as an MDP [35], as indexed by  $\mathcal{M} = \{\mathcal{W}, \mathcal{U}, \mathcal{P}, \mathcal{R}, \xi\}$ , where  $\mathcal{W}$  is the state space,  $\mathcal{U}$  is the action space,  $\mathcal{P}$  is the state transition probability from the current state to the next,  $\mathcal{R}$  is the reward function, and  $\xi$  is the discount factor. The following provides the definitions for all parameters.

The one-step reward  $r(x_{l,z}, u_{l,z})$  is defined as driving cost, which is associated with a particular action, as listed in (10).

$$r\left(x_{l,z}, u_{l,z}\right) = -\left(\zeta_e P_{b,z} + \zeta_t\right) \Delta t_z \tag{10}$$

We define  $\xi$  as an exponential decay factor so that long-term and short-term rewards can be balanced. Then, the  $\mathcal{R}(x_{l,z}, u_{l,z})$  is calculated by (11).

$$\mathcal{R}(x_{l,z}, u_{l,z}) = r(x_{l,z+1}, u_{l,z+1}) + \xi r(x_{l,z+2}, u_{l,z+2}) + \xi^2 r(x_{l,z+3}, u_{l,z+3}) + \dots$$
(11)

The state transition probability is defined by using the probability model  $\mathcal{P}\left(x_{l,z+1} \mid x_{l,z}, u_{l,z}\right) \in \{\mathcal{P}_{cl,z}, \mathcal{P}_{cr,z}, \mathcal{P}_{lk,z}\}$  for the predicted optimal driving costs  $C_{opt,z}$  and predicted actual driving costs (i.e.,  $C_{cl,z}$  and  $C_{cr,z}$  for left and right turning, respectively), as listed in (12) - (14), shown at the bottom of the next page, where  $\mathcal{P}_{cl,z}$ ,  $\mathcal{P}_{cr,z}$ , and  $\mathcal{P}_{lk,z}$  are the probabilities of changing lane to the left, changing lane to the right, and lane-keeping, respectively. It should be noted that improvements in energy efficiency for eco-driving often do not surpass 100% [4], thus we set the probability of lane-changing to 0 when actual driving cost surpasses optimal driving cost by a factor of two.

The  $C_{opt,z}$  is related to the feasible maximum time  $T_{pmax,z}$  and minimum time  $T_{pmin,z}$  to pass through the intersection.  $T_{pmax,z}$  and  $T_{pmin,z}$  can be calculated by considering the speed limits, vehicle position, and traffic light model [17]. Then,  $C_{opt,z}$  is calculated by using (15),

$$C_{opt,z} = \min \begin{bmatrix} \sum_{t_s}^{T_{pmin,z}} (\zeta_e P_b + \zeta_t) T_{pmin,z} \\ \sum_{t_s}^{T_{pmin,z} + \Delta t} (\zeta_e P_b + \zeta_t) (T_{pmin,z} + \Delta t) \\ \vdots \\ \sum_{t_s}^{T_{pmax,z}} (\zeta_e P_b + \zeta_t) T_{pmax,z} \end{bmatrix}$$
(15)

where  $t_s$  is the start time of the zth step, and  $\Delta t = 0.1$ s is the time interval. The actual driving costs depend on the driving operations and are affected by the movement of surrounding vehicles. Taking into account the impacts of stochastic traffic environments, this study proposes a heuristic driving cost prediction method. The proposed method divides the challenging task of evaluating the driving cost within a long horizon into two parts: present driving cost and foresighted driving cost,

as presented in (16)–(18),

$$C_{cl,z} = C_{clp,z} + C_{clf,z} \tag{16}$$

$$C_{cr,z} = C_{crp,z} + C_{crf,z} \tag{17}$$

$$C_{lk,z} = C_{lkp,z} + C_{lkf,z} \tag{18}$$

where  $C_{clp,z}$ ,  $C_{crp,z}$ , and  $C_{lkp,z}$  are the present driving costs for changing lane to the left, changing lane to the right, and lane-keeping, respectively, and  $C_{clf,z}$ ,  $C_{crf,z}$ , and  $C_{lkf,z}$  are the foresighted driving costs.

The present driving cost may be estimated more precisely since the traffic condition remains relatively constant for a short period. The costs of changing lanes to the left or right is the same, and the present driving costs can be calculated using (19) and (20).

$$C_{clp,z} = C_{crp,z} = \zeta_e P_b \Delta t_{c,z} + \zeta_t \Delta t_{c,z}$$
 (19)

$$C_{lkp,z} = \zeta_e P_b \Delta t_{k,z} + \zeta_t \Delta t_{k,z}$$
 (20)

In the calculation of foresighted driving costs, only the existing state of the preceding vehicle after the current driving lane selection operation is carried out, and the number of preceding vehicles is not evaluated. If the HV and the preceding vehicle do not collide, it is defined as lane-keeping mode; if the HV encounters the preceding vehicle upstream of the intersection, the timing and position of the encounter moment are estimated. In this situation, the HV will keep cruise-driving until encountering the preceding vehicle, and then follow the preceding vehicle. Therefore, the  $C_{clf,z}$ ,  $C_{crf,z}$ , and  $C_{lkf,z}$  are calculated using (21)–(23),

$$C_{clf,z} = \begin{cases} (\zeta_e P_b + \zeta_t) \left( t_{cdl,z} + t_{cfl,z} \right) & \vartheta = 1\\ (\zeta_e P_b + \zeta_t) & \frac{S_{tl} - \Delta s_{xc,z}}{V_{h,z}} & \vartheta = 0 \end{cases}$$
(21)

$$C_{crf,z} = \begin{cases} (\zeta_e P_b + \zeta_t) \left( t_{cdr,z} + t_{cfr,z} \right) & \vartheta = 1\\ (\zeta_e P_b + \zeta_t) & \frac{S_{tl} - \Delta s_{xc,z}}{V_{h,z}} & \vartheta = 0 \end{cases}$$
(22)

$$C_{lkf,z} = (\zeta_e P_b + \zeta_t) \frac{S_{tl} - \Delta s_{xk,z}}{V_{b,z}}$$
(23)

where  $\vartheta$  is the existing state of the preceding vehicle,  $\vartheta =$ 1 denotes that existing the preceding vehicle on the target lane, and HV can encounter the preceding vehicle before it reaches the intersection stop line; on the contrary,  $\vartheta = 0$  denotes the absence of the preceding vehicle or the preceding vehicle moving faster than HV.  $t_{cdl,z}$  and  $t_{cdr,z}$  are the cruise-driving time when HV catches up with the preceding vehicle by changing lanes to the left or right, respectively.  $t_{cfl,z}$  and  $t_{cfr,z}$  are the time of car-following after encounters preceding vehicles by changing lanes to the left or right, respectively.

The derivation for changing lanes to the left is demonstrated in the following; as the derivation for changing lanes to the right is identical, it is omitted.  $t_{cdl,z}$  and  $t_{cfl,z}$  are calculated using (24) and (25), respectively,

$$t_{cdl,z} = \begin{cases} \frac{d_{hp,z}}{V_{h,z} - V_{p,z}} & \text{if } T_{cpl,z} > \frac{d_{hp,z}}{V_{h,z} - V_{p,z}} \\ 0 & \text{others} \end{cases}$$
(24)

$$t_{cfl,z} = \begin{cases} \frac{S_{tl} - \Delta s_{xc,z} - V_{h,z} t_{cdl,z}}{V_{p,z}} & \text{if } T_{cpl,z} > \frac{d_{hp,z}}{V_{h,z} - V_{p,z}} \\ 0 & \text{others} \end{cases}$$

where  $d_{hp,z}$  is the distance between HV and the preceding vehicle,  $T_{cpl,z} = \left(S_{tl} - s_{xp,z} - V_{p,z} \Delta t_{c,z}\right) / V_{p,z}$  is the time for the preceding vehicle to pass through the intersection.  $V_{p,z}$ and  $s_{xp,z}$  are the speed and position of the preceding vehicle, respectively.

Then, the optimal solution of value function  $V(x_{l,z})$  and control policy  $\pi$  ( $x_{l,z}$ ) satisfies (26) and (27).

$$V\left(x_{l,z}\right) = \max_{u_{l,z} \in U} \mathcal{R}\left(x_{l,z}, u_{l,z}\right) + \sum_{x_{l,z+1}} \mathcal{P}\left(x_{l,z+1} \mid x_{l,z}, u_{l,z}\right) \mathcal{V}\left(x_{l,z+1}\right)$$

$$\pi\left(x_{l,z}\right) = \operatorname*{argmax}_{u_{l,z} \in U} \mathcal{R}\left(x_{l,z}, u_{l,z}\right)$$

$$(26)$$

$$+ \sum_{xl,z+1} \mathcal{P}(x_{l,z+1} | x_{l,z}, u_{l,z}) \mathcal{V}(x_{l,z+1})$$
(27)

Dynamic programming is utilized to resolve the MDP problem [36] and determine the optimal driving lane  $\mathcal{L}_{opt,z}$ .

## B. Energy-Saving Speed Optimization

1) Speed Optimization Problem: To get a real-time analytical solution, the speed optimization problem is formulated in (28) based on some assumptions. We define the driveline and battery system efficiencies as constant, i.e.,  $\eta_t = 0.9$  and  $\eta_b = 0.9$  [37]. In urban traffic, the vehicle moves at modest speeds to generate less air resistance, therefore air resistance is ignored [38]. In addition, as urban roads are often level, this study does not evaluate the impact of road slopes. To ensure a viable initial state, we assume the state constraints are inactive

$$\mathcal{P}_{cl,z} = \begin{cases}
\frac{C_{cl,z} - C_{opt,z}}{C_{cl,z} + C_{cr,z} + C_{lk,z} - 3C_{opt,z}} & \psi_{cl,z} = 1 \text{ and } C_{cl,z} < 2C_{opt,z} \\
0 & \psi_{cl,z} = 0 \text{ or } C_{cl,z}(z) \ge 2C_{opt,z}
\end{cases}$$

$$\mathcal{P}_{cr,z} = \begin{cases}
\frac{C_{cr,z} - C_{opt,z}}{C_{cl,z} + C_{cr,z} + C_{lk,z} - 3C_{opt,z}} & \psi_{cr,z} = 1 \text{ and } C_{cr,z} < 2C_{opt,z} \\
0 & \psi_{cr,z} = 0 \text{ or } C_{cr,z} \ge 2C_{opt,z}
\end{cases}$$
(12)

$$\mathcal{P}_{cr,z} = \begin{cases} \frac{C_{cr,z} - C_{opt,z}}{C_{cl,z} + C_{cr,z} + C_{lk,z} - 3C_{opt,z}} & \psi_{cr,z} = 1 \text{ and } C_{cr,z} < 2C_{opt,z} \\ 0 & \psi_{cr,z} = 0 \text{ or } C_{cr,z} > 2C_{opt,z} \end{cases}$$
(13)

$$\mathcal{P}_{lk,z} = 1 - \mathcal{P}_{cl,z} - \mathcal{P}_{cr,z} \tag{14}$$

at the beginning.

$$\min_{u_s \in U} \mathcal{J}_s(x, u_s) = \int_t^t \int_t^t \left\{ \left( \varpi v u_s + \kappa u_s^2 \right) \eta_b + \frac{P_a}{\eta_b} \right\} \zeta_e dt$$
subject to:  $\dot{s_x} = v, \dot{v} = \frac{u_s \dot{i}_g \dot{i}_0 \eta_t}{m \delta r_w} - \frac{gf}{\delta}, (6a), (6b)$ 
given:  $x(t_s) = [v_s, s_s]^T, s(t_f) = s_f$  (28)

where  $u_s$  is the control input, that is,  $u_s = T_m$ .  $t_s$  is the initial time of the current step,  $t_f$  is the estimated intersection passing time calculated using (24) and (25).

2) Analytical Solution Using PMP Algorithm: Different types of constraints are included in the speed optimization problem. According to the PMP solution criteria, the unconstrained solution is formed first, which is the basis to derive a constrained solution. The Hamiltonian in the unconstrained condition is given as (29),

$$H(x, u_s, t) = \left\{ \left( \varpi v u_s + \kappa u_s^2 \right) \eta_b + \frac{P_a}{\eta_b} \right\} \zeta_e + \phi_p v$$
$$+ \frac{\phi_s}{\delta} \left( \frac{u_s i_g i_0 \eta_t}{m r_m} - g f \right)$$
(29)

where  $\phi_p$  and  $\phi_s$  are the position and speed co-state variables, respectively. Following the *Euler-Lagrange* theory, the necessary conditions for optimality are given in (30)–(32).

$$\frac{\partial H}{\partial u_s} = (\varpi v + 2\kappa u_s) \eta_b \zeta_e + \frac{\phi_s i_g i_0 \eta_t}{m \delta r_w} = 0$$
 (30)

$$\frac{\partial H}{\partial x} = -\dot{\phi_p} = 0 \tag{31}$$

$$\frac{\partial H}{\partial v} = -\dot{\phi_s} = \varpi \, \eta_b \zeta_e u_s + \phi_p = 0 \tag{32}$$

Since  $\dot{\phi_p} = 0$  yields  $\phi_p$ ,  $v = v_s + \left(\frac{u_s i_g i_0 \eta_t}{m \delta r_w} - \frac{gf}{\delta}\right) t$ , and  $u_s = -\frac{\phi_p}{\varpi \eta_b \xi_e}$  (from (32),  $\dot{\phi_s} = 0$  when  $t = t_f$ ), the optimal control input  $u_s^*$ , speed  $v^*$ , and longitudinal position  $s_x^*$  can be calculated by using vehicle dynamics and (30)–(32), as shown in (33)–(35),

$$u_s^* = \Lambda_a t + \Lambda_b \tag{33}$$

$$v^* = \frac{\Lambda_a i_g i_0 \eta_t}{2m \delta r_w} t^2 + \left(\frac{\Lambda_b i_g i_0 \eta_t}{m r_w} - gf\right) \frac{t}{\delta} + e_v \tag{34}$$

$$s_x^* = \frac{\Lambda_a i_g i_0 \eta_t}{6m\delta r_w} t^3 + \left(\frac{\Lambda_b i_g i_0 \eta_t}{mr_w} - gf\right) \frac{t^2}{2\delta} + e_v t + e_s \quad (35)$$

with

$$\Lambda_{a} = \frac{1}{2\kappa\delta} \left( \varpi g f + \frac{\phi_{p} i_{g} i_{0} \eta_{t}}{m r_{w} \eta_{b} \zeta_{e}} \right)$$

$$\Lambda_{b} = -\frac{1}{2\kappa} \left( \varpi v_{s} + \frac{\phi_{s} i_{g} i_{0} \eta_{t}}{m \delta r_{w} \eta_{b} \zeta_{e}} \right)$$

where  $e_v$  and  $e_s$  are the constants of integration, which are determined by boundary conditions.

The optimal solution, which respects the speed and control constraints, can be obtained from the unconstrained optimal solution. Since the speed limits are pure state inequality constraints that are independent of the control input, we adjoin them in the *Hamiltonian* using the indirect method [39], which adjoins the  $p^{th}$  order state constraint indirectly up until the

control input is explicitly present. As a result, the explicit control input for the speed limits has to be included in one differential computation. As such, we define  $A^{(p)}(x, u_s, t)$  as the adjoining function of speed and control input constraints, as expressed in (36)–(39).

$$A_1^{(1)}(x, u_s, t) = \frac{1}{\delta} \left( \frac{u_s i_g i_0 \eta_t}{m r_w} - g f \right)$$
 (36)

$$A_2^{(1)}(x, u_s, t) = -\frac{1}{\delta} \left( \frac{u_s i_g i_0 \eta_t}{m r_w} - g f \right)$$
 (37)

$$A_3^{(0)}(x, u_s, t) = u_s - T_{mmax}$$
 (38)

$$A_{4}^{(0)}(x, u_{s}, t) = T_{mmin} - u_{s}$$
(39)

The resulting *Lagrangian* is formed as (40),

$$L(x, u_s, t) = H(x, u_s, t) + \varphi_1 A_1^{(1)}(x, u_s, t) + \varphi_2 A_2^{(1)}(x, u_s, t)$$
  
+  $\xi_1 A_3^{(0)}(x, u_s, t) + \xi_2 A_4^{(0)}(x, u_s, t)$  (40)

where  $\varphi$  and  $\xi$  are the co-states of speed and control input constraints. Note that the values of  $\varphi$  and  $\xi$  are always zero when the speed and control input constraints are not active, but they are not zero when the constraints are triggered.

Considering  $A^{(p)}(x, u_s, t) \leq 0$  does not prevent the speed and torque trajectories from exceeding the boundaries, then, the tangency conditions [40] of  $p^{th}$  order state constraints at the junction time must be added, as defined in (41),

$$B(x, u_s, t) = \begin{bmatrix} v(\tau) - V_{max} \\ V_{min} - v(\tau) \\ u_s(\tau) - T_{mmax} \\ T_{mmin} - u_s(\tau) \end{bmatrix} = 0$$
 (41)

where  $\tau$  is the entry time of the constraint.

The jump conditions derived from interior-point constraints at each relevant moment are defined in (42)–(44),

$$\phi_p^* (\tau^-) - \phi_p^* (\tau^+) = \sum_{j=0}^{p-1} \pi_j G_{x^*}^{(j)} (x^*, \tau)$$
 (42)

$$\phi_s^* \left( \tau^- \right) - \phi_s^* \left( \tau^+ \right) = \sum_{j=0}^{p-1} \pi_j G_{x^*}^{(j)} \left( x^*, \tau \right)$$
 (43)

$$H\left(\tau^{-}\right) - H\left(\tau^{+}\right) = \sum\nolimits_{j=0}^{p-1} \pi_{j} G_{t}^{(j)}\left(x^{*}, \tau\right) \tag{44}$$

where  $\pi_j$  is a *Lagrange* multiplier determined to satisfy constraints, and  $\tau^-$  and  $\tau^+$  are the time instances just before and after time  $\tau$ . Our previous research has revealed that the position co-state, speed co-state, *Hamiltonian*, and control input are continuous at  $t = \tau$  when the states and control input constraints are triggered independently [41].

Let  $\mathcal{F}$  be the constraint violated flag set, consisting of four bits representing the states of maximum speed, minimum speed, maximum control input, and minimum control input constraints, respectively. A value of 1 indicates that the constraint has been activated, while a value of 0 indicates that it has not. For example,  $\mathcal{F} = [1, 0, 0, 0]$  indicates that only the maximum speed constraint is activated. Then, the closed-form analytical solution of each state and control input constraints activation at  $t \in [t_1, t_2]$  for the optimal control input  $u_s^*$ , states  $(v^*$  and  $s_x^*$ ), and co-state variables  $(\varphi_1, \varphi_2, \xi_1, \xi_2)$ 

are calculated by (45)–(48).

$$u_{s}^{*} = \begin{cases} \frac{mgf\delta r_{w}}{ig^{i}0\eta_{t}} & \mathcal{F} = [1,0,0,0] \\ \frac{mgf\delta r_{w}}{ig^{i}0\eta_{t}} & \mathcal{F} = [0,1,0,0] \\ T_{mmax} & \mathcal{F} = [0,0,1,0] \\ T_{mmin} & \mathcal{F} = [0,0,0,1] \end{cases}$$

$$\begin{cases} \varphi_{1} = -\frac{m\delta r_{w}\eta_{b}\zeta_{e} (\varpi v + 2\kappa u_{s})}{ig^{i}0\eta_{t}} - \phi_{s} & \mathcal{F} = [1,0,0,0] \\ \varphi_{2} = \frac{m\delta r_{w}\eta_{b}\zeta_{e} (\varpi v + 2\kappa u_{s})}{ig^{i}0\eta_{t}} + \phi_{s} & \mathcal{F} = [0,1,0,0] \\ \xi_{1} = -\eta_{b}\zeta_{e} (\varpi v + 2\kappa u_{s}) - \frac{\phi_{s}ig^{i}0\eta_{t}}{m\delta r_{w}} & \mathcal{F} = [0,0,1,0] \\ \xi_{2} = \eta_{b}\zeta_{e} (\varpi v + 2\kappa u_{s}) + \frac{\phi_{s}ig^{i}0\eta_{t}}{m\delta r_{w}} & \mathcal{F} = [0,0,0,1] \end{cases}$$

$$v^{*} = \begin{cases} V_{max} & \mathcal{F} = [1,0,0,0] \\ V_{min} & \mathcal{F} = [0,1,0,0] \\ \left(\frac{ig^{i}0\eta_{t}T_{mmax}}{mr_{w}} - gf\right)\frac{t}{\delta} + e_{v} & \mathcal{F} = [0,0,0,1] \end{cases}$$

$$\left(\frac{ig^{i}0\eta_{t}T_{mmin}}{mr_{w}} - gf\right)\frac{t}{\delta} + e_{v} & \mathcal{F} = [0,0,0,1] \end{cases}$$

$$s_{x}^{*} = \begin{cases} V_{max} (t_{2} - t_{1}) + e_{s} & \mathcal{F} = [1, 0, 0, 0] \\ V_{min} (t_{2} - t_{1}) + e_{s} & \mathcal{F} = [0, 1, 0, 0] \\ \left(\frac{i_{g} i_{0} \eta_{t} T_{mmax}}{m r_{w}} - gf\right) \frac{t^{2}}{2\delta} + e_{s} & \mathcal{F} = [0, 0, 1, 0] \\ \left(\frac{i_{g} i_{0} \eta_{t} T_{mmin}}{m r_{w}} - gf\right) \frac{t^{2}}{2\delta} + e_{s} & \mathcal{F} = [0, 0, 0, 1] \end{cases}$$

$$(48)$$

Typically, the unconstrained optimal solution is calculated first, and the speed optimization problem is then solved by combining the solutions to the constrained and unconstrained problems if the unconstrained optimal solution violates any of the constraints. The procedure is continued until no more constraints are triggered by the solution. However, the large number of repeated calculations raises the computational cost. In this context, the active conditions of state and control input constraints are implemented based on the findings of Dong et al. [41] and Mahbub and Malikopoulos [42], to eliminate some constraints. For example, the control constraints only exist in the first phase of the optimal control sequence. Therefore, only state constraints rather than control input constraints may be activated later if the initial phase focuses on the unconstrained optimal solution.

The optimal control sequence depends on the order in which the vehicle state and control constraints are activated. For each case, the optimal control input, states, and entry time yield a set of two-point boundary value problem algebraic equations, which must be simultaneously solved while considering all constraints. Finally, a series of control input and states variable (i.e.,  $u_s^*$ ,  $v^*$ , and  $s_s^*$ ) within the prediction horizon can be obtained by using PMP in each receding optimization.

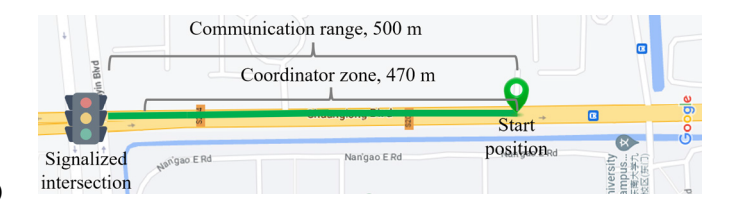


Fig. 5. Map of test route.

TABLE I VEHICLE PARAMETERS

Parameter	Value	Parameter	Value
Air density $\rho$	1.206kg/m <sup>3</sup>	Motor loss coefficient $M_2$	0.873
Air drag coefficient $C_D$	0.3	Rotational inertia $\delta$	1.022
Auxiliary power $P_a$	300W	Rolling resistance f	0.015
Front area A	$2.02m^{2}$	Tire radius $r_w$	0.280m
Final drive ratio $i_0$	3.789	Transmission ratio $i_g$	2.80
Gravity acceleration $g$	$9.8 \text{m/s}^2$	Vehicle mass m	1005kg
Maximum acceleration $a_{max}$	$2\text{m/s}^2$	Motor maximum propulsion torque $T_{mmax}$	67Nm
Maximum deceleration $a_{min}$	-2m/s <sup>2</sup>	Motor maximum generation torque $T_{mmin}$	-44Nm

In summary, in the *z*th receding optimization, the optimal control  $\mathcal{T}_{opt,z}$ , speed  $\mathcal{V}_{opt,z}$ , longitudinal position  $\mathcal{S}_{xopt,z}$ , lateral position  $\mathcal{S}_{yopt,z}$  are derived based on the  $\mathcal{L}_{opt,z}$ . During the lane-changing process,  $\mathcal{V}_{opt,z} = \mathcal{V}_{h,z}$ ,  $\mathcal{T}_{opt,z} = mgfr_w/i_gi_0\eta_t$ , and  $\mathcal{S}_{xopt,z}$  and  $\mathcal{S}_{yopt,z}$  are calculated by using vehicle kinematics and lane-changing trajectory models. In the lane-keeping process, the lateral position is not changed, therefore  $\mathcal{S}_{yopt,z} = 0$ . The derived optimal control input and state variables at the first step are then applied, that is,  $\mathcal{T}_{mopt,z} = u_s^*(1)$ ,  $\mathcal{V}_{opt,z} = v^*(1)$ , and  $\mathcal{S}_{xopt,z} = s_x^*(1)$ .

## V. SIMULATION AND RESULTS

# A. Simulation Setup

The vehicle parameters are taken from the Chery Little-Ant, as listed in Table I. Note that the motor maximum propulsion and generation torque are determined by considering the maximum acceleration/deceleration [43], speed limits, the motor torque bounds, and vehicle longitudinal dynamics. Referring to Pan et al. [44], the coefficients that convert the energy consumption and travel time into the monetary counterpart are 0.12USD/kWh and 24USD/hour, respectively. The traffic system is simulated using the real-world urban route as shown in Fig. 5, i.e., the intersection of Shuanglong Avenue and Jiyin Avenue, Nanjing, China, with the parameters listed in Table II. The intelligent driver model is employed as the car-following model to imitate the driving behavior of surrounding vehicles, and the LC2013 model is used to simulate vehicle lane-changing decisions [45]. The simulation is performed in MATLAB (version 9.13, 2022b) on a PC with Intel Core i9-12900k @ 3.20GHz CPU and 64GB RAM. The sampling time is 0.01s in simulation.

# B. Benchmark Strategy

To evaluate the performance of the OEAC, the constant speed (CS) and READ strategies are used as benchmarks. In a

TABLE II ROADWAY NETWORK AND TRAFFIC PARAMETERS

Parameter	Value	Parameter	Value
Communication range $D_{cr}$	500m	Road slope $\theta$	0
Coordinator zone $D_{lr}$	470m	Standstill distance $H_s$	2m
Location of stop line $S_{tl}$	500m	Safety time headway $T_h$	1.25s
Maximum speed $V_{max}$	70km/h	Time of red signal $T_{gr}$	51s
Minimum speed $V_{min}$	20km/h	Time of green signal $T_{gr}$	35s
Number of lanes $N_l$	3	Width of lane $D_w$	3.5m

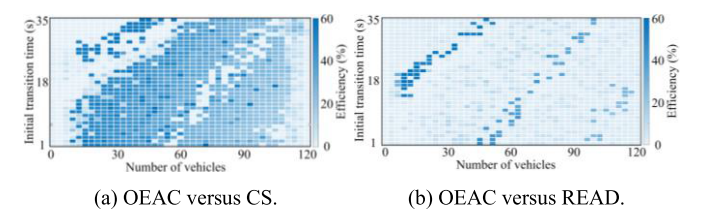


Fig. 6. Heat map of driving cost reduction of stochastic simulations, here the initial indication of the traffic light is green.

free-driving situation, the CS generally maintains a constant speed for the vehicle [13]. In addition, the READ generates an energy-efficient speed profile using the PMP algorithm while only considering lane-keeping operation [41]. When a preceding vehicle appears in front of the HV, the car-following strategy is activated in both CS and READ to keep a safe distance. The car-following driving behavior is modeled by the intelligent driver model.

# C. Simulation Results

1) Performance Verification in Stochastic Traffic Scenarios: The stochastic simulation is conducted to evaluate the driving cost reduction effectiveness of OEAC. The HV is initially located in the middle lane, and 10000 individual simulation trials are conducted with constant  $S_{tl}$ ,  $D_{cr}$ ,  $D_{lr}$ ,  $V_{min}$ ,  $V_{max}$ ,  $T_{gr}$ , and  $T_{re}$ . The parameters of the HV initial speed, traffic light initial states (i.e.,  $I_{in}$  (0 or 1) and  $T_{ls}$  (1– $T_{gr}$  or 1– $T_{re}$ )), traffic flow conditions (i.e., vehicle density (0–240veh/km), and initial position and speed of surrounding vehicles are all randomized in the simulation for a thorough investigation. Note that  $V_s$  is equal to the average traffic flow speed and is related to vehicle density.

The heat maps of the driving cost reduction of stochastic tests are depicted in Figs. 6 and 7. We point out that each grid of the heat map represents the average improvement of the different traffic scenarios with various speeds and positions of surrounding vehicles. Table III compares the driving cost reduction and computational time of the OEAC in each step.

Figs. 6 and 7 display the distribution of driving cost reduction for the OEAC under various traffic conditions. The minimum and maximum driving cost reduction of the OEAC are 0% and 59.97%, respectively, when compared to the CS. In comparison to the READ, the OEAC can cut the driving cost usage by up to 59.02%. On average, the OEAC performs significantly better than the CS and READ, achieving a driving cost reduction of 20.91% and 5.62%, respectively. The findings

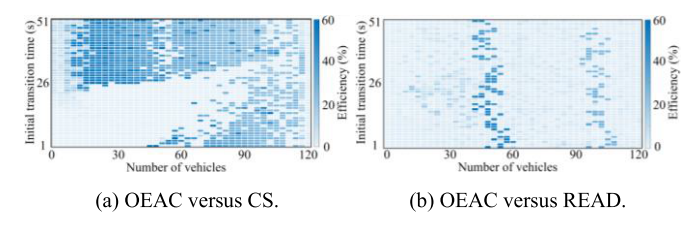


Fig. 7. Heatmap of driving cost reduction of stochastic simulations, here the initial indication of the traffic light is red.

TABLE III
RESULTS OF STOCHASTIC SIMULATION

Street enime	Driving cost reduction			Computational	
Strategies	Minimum	Maximum	Average	time in each step of OEAC	
OEAC versus CS	0%	59.97%	20.91%	0.2ms (average)	
OEAC versus READ	0%	59.02%	5.62%	9.3ms (maximum)	

TABLE IV
PARAMETERS OF THREE TYPICAL CASES

Parameters	Case A	Case B	Case C
Vehicle density	8veh/km	108veh/km	240veh/km
Average speed of traffic flow	70km/h	48km/h	20km/h
Initial transition time of traffic light	35s	20s	20s
Initial indication of traffic light	Green	Red	Green

indicate that the OEAC is remarkably effective in urban traffic. Although the driving cost reduction is similar to that of CS and READ in some scenarios, in most situations, the OEAC can effectively lower the driving cost. In addition, the initial states of traffic lights and traffic flow conditions have an impact on how well the OEAC performs in terms of reducing driving costs. Further investigation into this will be conducted below

Furthermore, as shown in Table III, the average and maximum computational time in each step of the OEAC are 0.2ms and 9.3ms, respectively, both of which are less than the sampling time (10ms). These results show that the proposed OEAC is computationally efficient and has the potential to be deployed in real-time.

2) Typical Cases Analysis: The stochastic simulation results allow for the selection of three typical cases with different vehicle density conditions: Cases A (free-flow), B (moderate-flow), and C (congested-flow). Table IV lists the parameters of three cases. A typical case analysis is then conducted to show the vehicle driving trajectories of three control strategies, enabling the further demonstration of the driving cost reduction by the OEAC. Figs. 8–10 show the vehicle speed, position, driving lane, and acceleration trajectories in three cases. Table V provides the vehicle driving cost, travel time, and energy consumption data for the OEAC and benchmark strategies. For a fair comparison, the energy consumption includes kinetic energy change between the starting and final positions and battery energy usage.

As illustrated in Fig. 8 and Table V, all three strategies enable HV to reach the destination without the need for lane

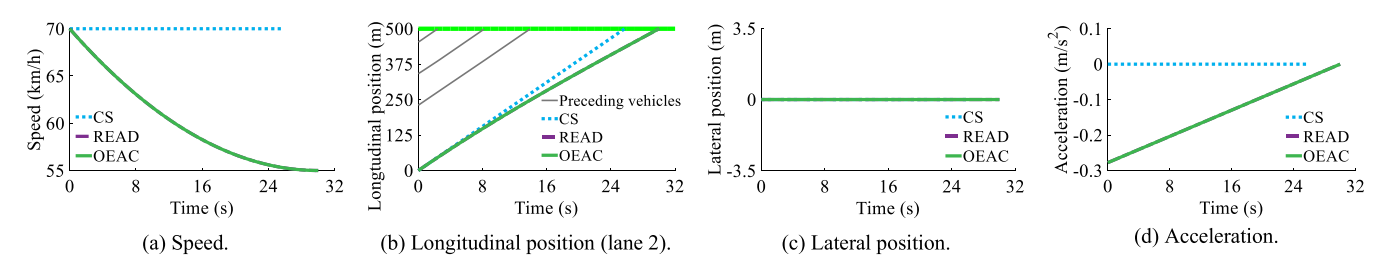


Fig. 8. Simulation results of Case A. Here, the HV keeps driving in lane 2 of CS, READ, and OEAC strategies.

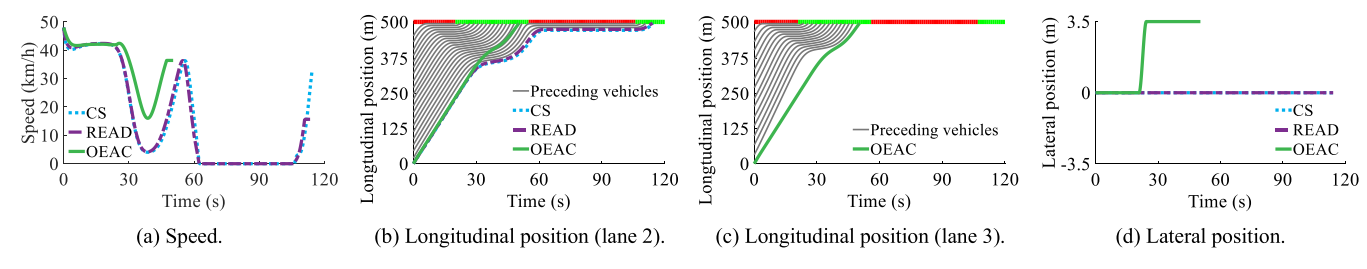


Fig. 9. Simulation results of Case B. Here, the HV keeps driving in lane 2 firstly and changes to lane 3 at 20.91s of OEAC strategy, and keeps driving in lane 2 of the CS and READ strategies.

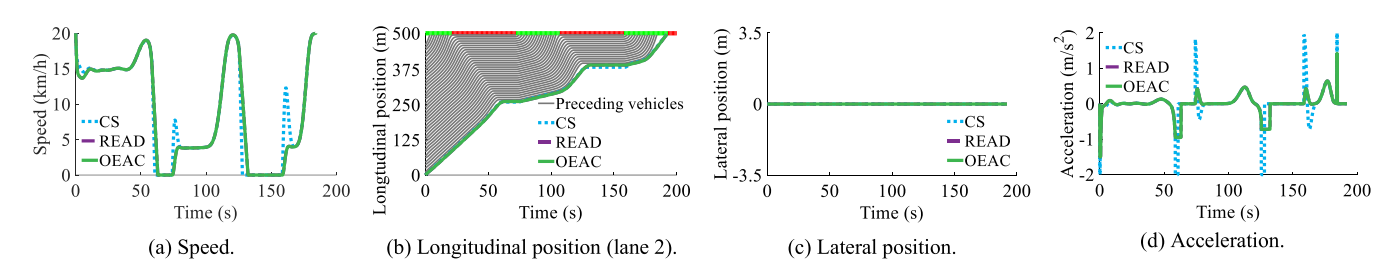


Fig. 10. Simulation results of Case C. Here, the HV keeps driving in lane 2 of CS, READ, and OEAC strategies.

 $\label{eq:table V} \textbf{TABLE V}$  Simulation Results of Three Typical Cases

Parame	ters	Case A	Case B	Case C
Driving cost	CS	0.24USD	0.85USD	1.37USD
	READ	0.23USD	0.83USD	1.36USD
	OEAC	0.23USD	0.39USD	1.36USD
Travel time	CS	25.80s	114.30s	191.71s
	READ	30.02s	114.20s	192.01s
	OEAC	30.02s	50.37s	192.01s
Energy consumption	CS	202.95kJ	305.41kJ	279.17kJ
	READ	162.59kJ	283.26kJ	263.73kJ
	OEAC	162.59kJ	194.15kJ	263.73kJ

change operations (Fig. 8(c)), while also remaining unaffected by preceding vehicles. As a consequence, both OEAC and READ strategies yield the same solution. Although OEAC and READ have longer travel times compared to the CS, they save vehicle energy consumption. When compared with the CS strategy, the OEAC and READ can reduce the driving cost by 4.17%. This is due to the capacity of OEAC and READ to leverage traffic light information to optimize smoothly changing speed and acceleration (see Figs. 8(a) and 8(d)) so that the HV passes through the signalized intersection at the

least driving cost. According to the findings, the OEAC offers no benefit over the READ and provides only a slight driving cost reduction over the CS in the free-flow traffic condition due to the nature of this situation.

Fig. 9 illustrates that both the CS and READ need the controlled HV to pass through the signalized intersection at the second traffic light green signal window (see Fig. 9(b)) because the preceding vehicles hinder the movement of HV. As a result, see Table V, the driving cost of CS and READ increases as vehicle energy usage and travel time rise. In contrast, the OEAC changes the driving lane from lane 2 to lane 3 (see Fig. 9(d)), allowing the HV to pass through the signalized intersection during the first traffic light green signal window (see Fig. 9(c)), thereby reducing the driving cost. Compared to the CS and READ, the OEAC effectively optimizes the vehicle driving lane and speed in moderate-flow conditions, resulting in a decrease of 55.93%/55.89%, 36.43%/31.46%, and 54.12%/53.01% in travel time, energy consumption, and driving cost, respectively. This reveals that the energy and travel time of the HV are more affected by the preceding vehicles in moderate-flow. The OEAC performs effectively in moderate-flow conditions by optimizing the vehicle driving lane and speed, lowering vehicle energy consumption and travel time to reduce driving costs.

In congested-flow conditions, as shown in Fig. 10, the HV with OEAC passes through the signalized intersection without

lane-changing operation. Because there are more vehicles on the road, the average speed of the traffic flow is slower, and the spacing between vehicles is smaller; hence, there is no appropriate lane-changing opportunity for HV to reduce travel time and energy consumption. The OEAC and READ strategies have identical driving trajectories, so their energy consumption, travel time, and driving cost are identical (see Table V).

3) Sensitive Analysis for the OEAC: According to the findings of the stochastic traffic scenarios simulation and typical case analysis, the effectiveness of OEAC is influenced by many factors. This subsection provides a comprehensive investigation of various factors that impact the performance improvement of OEAC, particularly concerning traffic flow conditions and initial states of traffic lights.

In free-flow conditions, HV is unaffected by the preceding vehicles in all lanes, then the probability of lane-changing of HV is 0. The OEAC and READ have the same performance and are better than CS. As shown in Fig. 9(b), the degree of OEAC's superiority over CS depends on the traffic light's initial states. For example, if the average traffic flow speed is 70km/h, HV arrives at the intersection at the 25.71s under CS control. As a result, if the initial indication is red, the HV has a stop-and-go operation at the intersection under CS control if the initial transition time exceeds 25.71s. However, OEAC can avoid the stop-and-go operation by optimizing the vehicle speed. Because the operation of stop-and-go consumes more energy, the energy efficiency of OEAC is preferable to CS. In addition, the travel time difference between OEAC and CS is small, as both are impacted by the initial traffic light states. Therefore, the advantage of OEAC over CS in driving cost reduction is mostly from the reduced energy usage brought about by the optimized free-driving speed. Consequently, in the free-flow condition, the effectiveness of OEAC results is due to speed optimization and is sensitive to traffic light initial states (see Figs. 6(a) and 7(a)).

In congested-flow conditions, the effectiveness of OEAC is similar to CS and READ as there is limited safe clearance for lane-changing due to slower preceding vehicles. In contrast to the free-flow condition, the effectiveness of OEAC over CS in the congested-flow condition is sensitive to the surrounding vehicle condition, because CS, READ, and OEAC strategies are all run in car-following mode (see Fig. 10(b)). The advantage of OEAC over CS in driving cost reduction is primarily due to the optimized car-following speed, which leads to lower energy. Thus, the driving cost reduction of OEAC over CS is more spread with different traffic light initial states, as shown in Figs. 6(a) and 7(a).

In moderate-flow conditions, the HV has more possibilities to change lane, hence the advantage of OEAC is obvious in reducing driving costs. Under the control of OEAV, HV can choose the lane that allows for the fastest passage through the signalized intersection while optimizing the driving speed to reduce travel time and energy consumption. As shown in Figs. 6 and 7, the OEAC outperforms the CS and READ in terms of driving cost reduction in the vehicle density range of 20-220veh/km. In addition, the improvements are more uniformly distributed, as the probability of lane-changing is

sensitive to both the surrounding vehicle conditions and the initial states of traffic lights.

## VI. CONCLUSION

This study proposes an overtaking-enabled EAD control strategy for CAVs, namely OEAC, which efficiently reduces driving costs by combining driving lane planning and speed optimization. An overtaking-enabled EAD optimal control problem is formulated with unified monetary counterpart objectives of energy consumption and travel time while accounting for the traffic light and preceding vehicle constraints. The OEAC utilizes the two-stage receding horizon control framework to solve the optimal control problems in real-time, resulting in an optimal driving trajectory. In the first stage, the MDP theory is adopted to plan an efficient driving lane while accounting for the uncertain disturbance of preceding vehicles. In the second stage, the speed trajectory is optimized with the PMP algorithm to minimize driving costs with the minimized computational cost.

The stochastic traffic scenarios simulation and typical case study are investigated to verify the effectiveness of the OEAC. The results demonstrate that the OEAC outperforms CS and READ strategies in various traffic environments, with an average improvement of 20.91% and 5.62%, respectively. Furthermore, the sensitivity analysis findings manifest that OEAC's capability of lowering driving costs is mainly affected by the initial states of traffic lights in free flow, surrounding vehicle conditions in moderate flow, and both surrounding vehicle conditions and the initial states of traffic lights in congested flow.

Future research will incorporate robust optimization theory into a lane-changing enabled eco-driving control framework to take into account more uncertainty disturbance in terms of traffic, vehicle, pedestrian, and communication.

#### REFERENCES

- [1] B. Peng, M. F. Keskin, B. Kulcsár, and H. Wymeersch, "Connected autonomous vehicles for improving mixed traffic efficiency in unsignalized intersections with deep reinforcement learning," *Commun. Transp. Res.*, vol. 1, Dec. 2021, Art. no. 100017.
- [2] M. Zhu et al., "Public vehicles for future urban transportation," *IEEE Trans. Intell. Transp. Syst.*, vol. 17, no. 12, pp. 3344–3353, Dec. 2016.
- [3] J.-L. Fan, J.-X. Wang, F. Li, H. Yu, and X. Zhang, "Energy demand and greenhouse gas emissions of urban passenger transport in the Internet era: A case study of Beijing," *J. Cleaner Prod.*, vol. 165, pp. 177–189, Nov. 2017.
- [4] A. Vahidi and A. Sciarretta, "Energy saving potentials of connected and automated vehicles," *Transp. Res. C, Emerg. Technol.*, vol. 95, pp. 822–843, Oct. 2018.
- [5] J. Zhu, S. Easa, and K. Gao, "Merging control strategies of connected and autonomous vehicles at freeway on-ramps: A comprehensive review," *J. Intell. Connected Vehicles*, vol. 5, no. 2, pp. 99–111, Dec. 2022.
- [6] H. Wang et al., "Network-wide traffic signal control using bilinear system modeling and adaptive optimization," *IEEE Trans. Intell. Transp.* Syst., vol. 24, no. 1, pp. 79–91, Jan. 2023.
- [7] H. Xia, Eco-Approach and Departure Techniques for Connected Vehicles at Signalized Traffic Intersections. Oakland, CA, USA: Univ. California, 2014.
- [8] P. Hao, G. Wu, K. Boriboonsomsin, and M. J. Barth, "Eco-approach and departure (EAD) application for actuated signals in real-world traffic," *IEEE Trans. Intell. Transp. Syst.*, vol. 20, no. 1, pp. 30–40, Jan. 2019.
- [9] K. Katsaros, R. Kernchen, M. Dianati, D. Rieck, and C. Zinoviou, "Application of vehicular communications for improving the efficiency of traffic in urban areas," *Wireless Commun. Mobile Comput.*, vol. 11, no. 12, pp. 1657–1667, Nov. 2011.

- [10] G. Mahler and A. Vahidi, "An optimal velocity-planning scheme for vehicle energy efficiency through probabilistic prediction of traffic-signal timing," *IEEE Trans. Intell. Transp. Syst.*, vol. 15, no. 6, pp. 2516–2523, Dec. 2014.
- [11] Z. Bai, P. Hao, W. ShangGuan, B. Cai, and M. J. Barth, "Hybrid reinforcement learning-based eco-driving strategy for connected and automated vehicles at signalized intersections," *IEEE Trans. Intell. Transp. Syst.*, vol. 23, no. 9, pp. 15850–15863, Sep. 2022.
- [12] F. Ye, P. Hao, X. Qi, G. Wu, K. Boriboonsomsin, and M. J. Barth, "Prediction-based eco-approach and departure at signalized intersections with speed forecasting on preceding vehicles," *IEEE Trans. Intell. Transp. Syst.*, vol. 20, no. 4, pp. 1378–1389, Apr. 2019.
- [13] H. Dong, W. Zhuang, B. Chen, G. Yin, and Y. Wang, "Enhanced ecoapproach control of connected electric vehicles at signalized intersection with queue discharge prediction," *IEEE Trans. Veh. Technol.*, vol. 70, no. 6, pp. 5457–5469, Jun. 2021.
- [14] C. Sun, C. Zhang, H. Yu, W. Liang, Q. Ren, and J. Li, "An eco-driving approach with flow uncertainty tolerance for connected vehicles against waiting queue dynamics on arterial roads," *IEEE Trans. Ind. Informat.*, vol. 18, no. 8, pp. 5286–5296, Aug. 2022.
- [15] Z. Wang, G. Wu, and M. J. Barth, "Cooperative eco-driving at signalized intersections in a partially connected and automated vehicle environment," *IEEE Trans. Intell. Transp. Syst.*, vol. 21, no. 5, pp. 2029–2038, May 2020.
- [16] J. Han, D. Shen, D. Karbowski, and A. Rousseau, "Leveraging multiple connected traffic light signals in an energy-efficient speed planner," *IEEE Control Syst. Lett.*, vol. 5, no. 6, pp. 2078–2083, Dec. 2021.
- [17] H. Dong et al., "Predictive energy-efficient driving strategy design of connected electric vehicle among multiple signalized intersections," *Transp. Res. C, Emerg. Technol.*, vol. 137, Apr. 2022, Art. no. 103595.
- [18] F. Ma et al., "Eco-driving-based cooperative adaptive cruise control of connected vehicles platoon at signalized intersections," *Transp. Res. D, Transp. Environ.*, vol. 92, Mar. 2021, Art. no. 102746.
- [19] S. Li, J. Li, J. Pei, S. Wu, S. Wang, and L. Cheng, "Eco-CSAS: A safe and eco-friendly speed advisory system for autonomous vehicle platoon using consortium blockchain," *IEEE Trans. Intell. Transp. Syst.*, vol. 24, no. 7, pp. 7802–7812, Jul. 2023, doi: 10.1109/TITS.2022.3232851.
- [20] X. Jiang, J. Zhang, X. Shi, and J. Cheng, "Learning the policy for mixed electric platoon control of automated and human-driven vehicles at signalized intersection: A random search approach," *IEEE Trans. Intell. Transp. Syst.*, vol. 24, no. 5, pp. 5131–5143, May 2023, doi: 10.1109/TITS.2023.3242678.
- [21] J. Zhou, H. Zheng, J. Wang, Y. Wang, B. Zhang, and Q. Shao, "Multiobjective optimization of lane-changing strategy for intelligent vehicles in complex driving environments," *IEEE Trans. Veh. Technol.*, vol. 69, no. 2, pp. 1291–1308, Feb. 2020.
- [22] Y. Li, L. Li, D. Ni, and W. Wang, "Automatic lane-changing trajectory planning: From self-optimum to local-optimum," *IEEE Trans. Intell. Transp. Syst.*, vol. 23, no. 11, pp. 21004–21014, Nov. 2022.
- [23] Z. Gu et al., "Integrated eco-driving automation of intelligent vehicles in multi-lane scenario via model-accelerated reinforcement learning," *Transp. Res. C, Emerg. Technol.*, vol. 144, Nov. 2022, Art. no. 103863.
- [24] H. Dong et al., "Flexible eco-cruising strategy for connected and automated vehicles with efficient driving lane planning and speed optimization," *IEEE Trans. Transport. Electrific.*, early access, Jun. 28, 2023, doi: 10.1109/TTE.2023.3289980.
- [25] R. Chen, C. G. Cassandras, A. Tahmasbi-Sarvestani, S. Saigusa, H. N. Mahjoub, and Y. K. Al-Nadawi, "Cooperative time and energyoptimal lane change maneuvers for connected automated vehicles," *IEEE Trans. Intell. Transp. Syst.*, vol. 23, no. 4, pp. 3445–3460, Apr. 2022.
- [26] J. Yang et al., "A less-disturbed ecological driving strategy for connected and automated vehicles," *IEEE Trans. Intell. Vehicles*, vol. 8, no. 1, pp. 413–424, Jan. 2023.
- [27] Q. Guo, O. Angah, Z. Liu, and X. Ban, "Hybrid deep reinforcement learning based eco-driving for low-level connected and automated vehicles along signalized corridors," *Transp. Res. C, Emerg. Technol.*, vol. 124, Mar. 2021, Art. no. 102980.
- [28] P. Bansal and K. M. Kockelman, "Forecasting Americans' long-term adoption of connected and autonomous vehicle technologies," *Transp. Res. A, Policy Pract.*, vol. 95, pp. 49–63, Jan. 2017.
- [29] H. Zhu, Z. Song, W. Zhuang, H. Hofmann, and S. Feng, "Multi-objective optimization for connected and automated vehicles using machine learning and model predictive control," SAE Int. J. Electrified Vehicles, vol. 11, no. 2, pp. 177–187, Nov. 2021.

- [30] J. Hu, Z. Zhang, L. Xiong, H. Wang, and G. Wu, "Cut through traffic to catch green light: Eco approach with overtaking capability," *Transp. Res. C, Emerg. Technol.*, vol. 123, Feb. 2021, Art. no. 102927.
- [31] J. Han, A. Sciarretta, L. L. Ojeda, G. De Nunzio, and L. Thibault, "Safeand eco-driving control for connected and automated electric vehicles using analytical state-constrained optimal solution," *IEEE Trans. Intell.* Vehicles, vol. 3, no. 2, pp. 163–172, Jun. 2018.
- [32] Y. Yan et al., "Eco-coasting controller using road grade preview: Evaluation and online implementation based on mixed integer model predictive control," *IEEE Trans. Veh. Technol.*, vol. 72, no. 10, pp. 12508–12523, Oct. 2023, doi: 10.1109/TVT.2023.3271656.
- [33] H. Dong et al., "Energy-optimal braking control using a double-layer scheme for trajectory planning and tracking of connected electric vehicles," Chin. J. Mech. Eng., vol. 34, no. 1, pp. 1–12, Dec. 2021.
- [34] M. Treiber, A. Hennecke, and D. Helbing, "Congested traffic states in empirical observations and microscopic simulations," *Phys. Rev. E, Stat. Phys. Plasmas Fluids Relat. Interdiscip. Top.*, vol. 62, no. 2, pp. 1805–1824, Aug. 2000.
- [35] R. Bellman, "A Markov decision process," J. Math. Mech., vol. 6, no. 5, pp. 679–684, 1957.
- [36] M. L. Puterman, Markov Decision Processes: Discrete Stochastic Dynamic Programming. Hoboken, NJ, USA: Wiley, 2014.
- [37] Y. Xie et al., "Microsimulation of electric vehicle energy consumption and driving range," Appl. Energy, vol. 267, Jun. 2020, Art. no. 115081.
- [38] J. Han, J. Rios-Torres, A. Vahidi, and A. Sciarretta, "Impact of model simplification on optimal control of combustion engine and electric vehicles considering control input constraints," in *Proc. IEEE Vehicle Power Propuls. Conf. (VPPC)*, Aug. 2018, pp. 1–6.
- [39] R. F. Hartl, S. P. Sethi, and R. G. Vickson, "A survey of the maximum principles for optimal control problems with state constraints," *SIAM Rev.*, vol. 37, no. 2, pp. 181–218, Jun. 1995.
- [40] B. Chalaki and A. A. Malikopoulos, "Optimal control of connected and automated vehicles at multiple adjacent intersections," *IEEE Trans. Control Syst. Technol.*, vol. 30, no. 3, pp. 972–984, May 2022.
- [41] H. Dong et al., "Event-driven energy-efficient driving control in urban traffic for connected electric vehicles," *IEEE Trans. Transport. Electrific.*, vol. 9, no. 1, pp. 99–113, Mar. 2023.
- [42] A. M. I. Mahbub and A. A. Malikopoulos, "Conditions to provable system-wide optimal coordination of connected and automated vehicles," *Automatica*, vol. 131, Sep. 2021, Art. no. 109751.
- [43] Y. Li, L. Zhao, K. Gao, Y. An, and J. Andric, "Revealing driver psychophysiological response to emergency braking in distracted driving based on field experiments," *J. Intell. Connected Vehicles*, vol. 5, no. 3, pp. 270–282, Dec. 2022.
- [44] T. Pan, R. Guo, W. H. K. Lam, R. Zhong, W. Wang, and B. He, "Integrated optimal control strategies for freeway traffic mixed with connected automated vehicles: A model-based reinforcement learning approach," *Transp. Res. C, Emerg. Technol.*, vol. 123, Feb. 2021, Art. no. 102987.
- [45] J. Erdmann, "Lane-changing model in SUMO," in *Proc. SUMO Model. Mobility Open Data*, vol. 24. Berlin, Deutschland: Deutsches Zentrum für Luft- und Raumfahrt e.V., 2014, pp. 77–88.



**Haoxuan Dong** received the Ph.D. degree in mechanical engineering from Southeast University, Nanjing, China, in 2022.

From February 2022 to June 2022, he was a Visiting Researcher with the Department of Architecture and Civil Engineering, Chalmers University of Technology, Gothenburg, Sweden. He is currently a Research Fellow with the Department of Mechanical Engineering, National University of Singapore, Singapore. His current research interests include connected and automated vehicles, energy-efficient

driving, and vehicle dynamics control. He was a recipient of the China SAE Outstanding Doctoral Dissertation Award in 2023.



Weichao Zhuang (Member, IEEE) received the B.S. and Ph.D. degrees in mechanical engineering from the Nanjing University of Science and Technology, Nanjing, China, in 2012 and 2017, respectively.

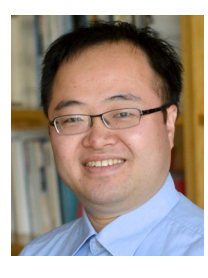
From 2014 to 2015, he was a Visiting Student with the Department of Mechanical Engineering, University of Michigan, Ann Arbor, MI, USA. He is currently an Associate Professor with the School of Mechanical Engineering, Southeast University, China. His current research interests include optimal control, clean energy vehicles, connected vehicles, and multi-agent control.



**Guodong Vin** (Senior Member, IEEE) received the Ph.D. degree in mechanical engineering from Southeast University, Nanjing, China, in 2007.

From August 2011 to August 2012, he was a Visiting Scholar with the Department of Mechanical and Aerospace Engineering, The Ohio State University, Columbus, OH, USA. He is currently a Chair Professor with the School of Mechanical Engineering, Southeast University. His research interests include connected and automated vehicles, vehicle dynamics and control, and advanced vehicle control. He was a

recipient of the National Science Fund for Distinguished Young Scholars of China. He is an Associate Editor of IEEE TRANSACTIONS ON INTELLIGENT VEHICLES.



**Guoyuan Wu** (Senior Member, IEEE) received the Ph.D. degree in mechanical engineering from the University of California at Berkeley, Berkeley, in 2010.

He is currently a Full Researcher and an Adjunct Professor with the Bourns College of Engineering–Center for Environmental Research and Technology (CE-CERT) and the Department of Electrical and Computer Engineering, University of California at Riverside. His research interests include the development and evaluation of sustain-

able and intelligent transportation system (SITS) technologies, connected and automated transportation systems (CATS), shared mobility, transportation electrification, optimization and control of vehicles, traffic simulation, and energy/emissions measurement and modeling. He is a member of the National Academy of Inventors (NAI) and the several Standing Committees of the Transportation Research Board (TRB). He was a recipient of the 2020 Vincent Bendix Automotive Electronics Engineering Award, the 2021 Arch T. Colwell Merit Award, and the 2017–2020 IEEE-ITSM Outstanding Survey Paper Award. He has serves as an Associate Editor for a few prestigious journals in the area of ITS.



Zhaojian Li (Senior Member, IEEE) received the M.S. and Ph.D. degrees in aerospace engineering (flight dynamics and control) from the University of Michigan, Ann Arbor, MI, USA, in 2013 and 2015, respectively. He was an Algorithm Engineer with General Motors from January 2016 to July 2017. He is currently a Red Cedar Distinguished Associate Professor with the Department of Mechanical Engineering, Michigan State University. He is the author of more than 50 top journal articles and several patents. His research interests include learning-based

control, nonlinear and complex systems, and robotics and automated vehicles. He was a recipient of the NSF CAREER Award. He is an Associate Editor of IEEE TRANSACTIONS ON INTELLIGENT VEHICLES, *Evolving Systems*, the American Control Conference, and the ASME Dynamics and Control Conference.



**Ziyou Song** (Senior Member, IEEE) received the B.E. and Ph.D. degrees (Hons.) in automotive engineering from Tsinghua University, Beijing, China, in 2011 and 2016, respectively.

After graduation, he was a Research Scientist with Tsinghua University from 2016 to 2017. From 2017 to 2019, he was a Post-Doctoral Research Fellow with the University of Michigan, Ann Arbor, MI, USA, where he was also an Assistant Research Scientist/Lecturer from 2019 to 2020. He is currently an Assistant Professor with the Department of

Mechanical Engineering, National University of Singapore. Prior to joining NUS, he was a Battery Algorithm Engineer with Apple Inc., Cupertino, CA, USA, where he was in charge of battery management systems for Audio products (e.g., AirPods). He is the author or coauthor of two book chapters and more than 80 peer-reviewed publications including 60 journal articles. His research interests include modeling, estimation, optimization, and control of energy storage (e.g., battery, supercapacitor, and flywheel) for electrified vehicles. Using energy storage as a bridge, his group is actively connecting the automotive, transportation, and power system communities by collaborating on interdisciplinary projects to ensure that both power system and transportation system are efficient, reliable, and clean. He received several paper awards, including the Applied Energy 2015-2016 Highly Cited Paper Award, the Applied Energy Award for Most Cited Energy Article from China, the NSK Outstanding Paper Award of Mechanical Engineering, and the 2013 IEEE VPPC Best Student Paper Award. He serves as a reviewer for more than 50 international journals. He also serves as an Associate Editor for Automotive Innovation, SAE International Journal of Electrified Vehicles, and IEEE TRANSACTIONS ON TRANSPORTATION ELECTRIFICATION.